Characteristics of Porous Tungsten Ionizers

O. K. HUSMANN* AND R. TURK†
Hughes Aircraft Company, Malibu, Calif.

An important characteristic of the electric propulsion system is its total efficiency: the product of power and ionization efficiency. A total efficiency of over 90% is desirable. High pore densities improve the ionization efficiency and reduce electrode erosion. Neutral efflux of 2.7% at 10 ma/cm² cesium ion current density is reported here for porous tungsten pellets as surface ionizers, coated with a thin layer of fine tungsten powder. Both coat and substrate pore density influence the neutral efflux, and pore densities exceeding 5×10^6 pores/cm² (line intercept method) are desirable. Neutral efflux measurements up to 25 ma/cm² ion current density are reported. Extrapolated measurements of the sintering rate of spherical tungsten powder as fine as 3.9 μ show it to be sufficiently stable for use at 1373°K for one year at densities of 80% or above. Change of direct pore count over one year is about 2%.

Introduction

POWER and ionization efficiency basically depend on the ion emitter performance. The minimum possible neutral flux and radiation loss are required. Earlier experiments showed ion emitter improvement with increasing pore density per unit surface area.[1] As a result, the past year's effort has been spent primarily on the development of high pore density ionizers. So far, two different types with increased pore densities have been produced, and their characteristics are discussed. One uses a coat of fine spherical tungsten powder on a low pore density tungsten substrate. The other is sintered from spherical tungsten in the low micron range. Pore densities exceeding 10^6 pores/cm² are available from both types. Neutral flux and critical temperature are improved in accordance with the counted pore densities. (For pore counting the traverse technique is applied.)

Development of High Pore Density Sintered Tungsten

A high pore density structure of tungsten is obtained by incomplete densification of fine powder during sintering. The number and uniformity of pores, pore size, and spacing are related directly to the size, uniformity, and initial packing of the original tungsten powder used for fabrication of the porous body.

Uniform, high pore density structures having 1.9×10^6 pores/cm² by line-intercept evaluation (more than 5×10^6 by direct count) have been produced at Hughes, using classified fractions of spherical tungsten powder in close-packed array as sintering material (Fig. 1). This porous tungsten is uniform in structure, reproducible, and free from localized sporadic grain growth. Interconnectability of the pores at the 82% density is over 99%. Thin slabs of this material, made by hot-pressing from 2.4 μ powder, have been prepared in sizes of $2.5 \times 4.25 \times \frac{1}{8}$ in. thick. The raw material was obtained by spheroidizing angular tungsten powder in a plasma arc, chemically removing surface oxide to reduce interparticle friction and permit close packing, and classifying into narrow size ranges for predictability and uniformity of final pore structure.

Two chief problems were encountered. Fabrication into large ionizer plates was difficult because of the low pressed strength of the clean, classified spherical powder, and stability of the resulting sintered structure was lower as the pore density increased (with use of finer powder).

The problem of low pressed strength was solved after thorough investigation of all of the conventional methods of consolidation, including uniaxial pressing, isostatic pressing, and gravity sintering. Without using contaminating binders or sacrificing the narrow size range of powders, a high pressed strength was obtained by warm-pressing the powder at 300°C for 30 min at a pressure of 75,000 psi. This technique permits economical use of expensive separated powders, since thin plates close to final size are pressed. In addition, the pressed density of 74% indicates almost perfect packing of spheres, yielding the maximum pore density for a given powder size. The method permits control of uniformity of density/porosity since the die fill may be leveled and "combed" many times to insure uniform density before pressing which is so essential to uniformity of the product.

Vacuum sintering of the pressed slab is controlled to give a density close to 80% of theoretical, and copper is infiltrated into the piece prior to machining. Copper infiltration into a piece free from any trace of oxide is so complete that it may be used as a measure of pore interconnectability.

The stability of the final ionizer structure is dependent upon the initial particle size, since the higher surface area of finer powders leads to more rapid sintering. Removal of fine powders below 0.5 to 1 μ gives added stability to powders as fine as 2.4 μ. In addition, the spherical shape, which has less surface area, is more stable than the angular and cubic shapes associated with commercial hydrogen-reduced tungsten powders.

Since very high pore density and long-term high-temperature structural stability are mutually exclusive, intelligent choice of an optimum ionizer material requires that both ionization efficiency (a function of pore count) and sintering stability be known.

Sintering kinetics studies at Hughes have yielded data for predicting long-term structural stability at ionizer temperatures from results of sintering tests at high temperatures for shorter times. Results of initial tests of spherical tungsten powders at mean diameters of 3.9 and 6.9 μ are presented in Fig. 2. A 3.3-μ spherical tungsten powder is shown in Fig. 1, along with its normal distribution. Plotted is the relative frequency vs grain size. The standard deviation is 0.6μ. A typical resultant sintered structure cross section is below the distribution curve.

Sintering was conducted in vacuum (10^{-6} torr) at temperatures from 1773° to 2573°K and for times of 20 to 480 min (Fig. 2). It should be noted that considerably higher temperatures were used to attain similar density changes in the 6.9-μ material (dashed lines) as opposed to those used for the 3.9-μ material (solid lines).

Presented as Preprint 64-691 at the AIAA Fourth Electric Propulsion Conference, Philadelphia, Pa., August 31-September 2, 1964; revision received May 7, 1965. This work was conducted under Contract No. NAS 3-4110.

* Senior Member of the Technical Staff, Hughes Research Laboratories. Member AIAA.

† Member of the Technical Staff, Metallurgist, Hughes Research Laboratories. Member AIAA.

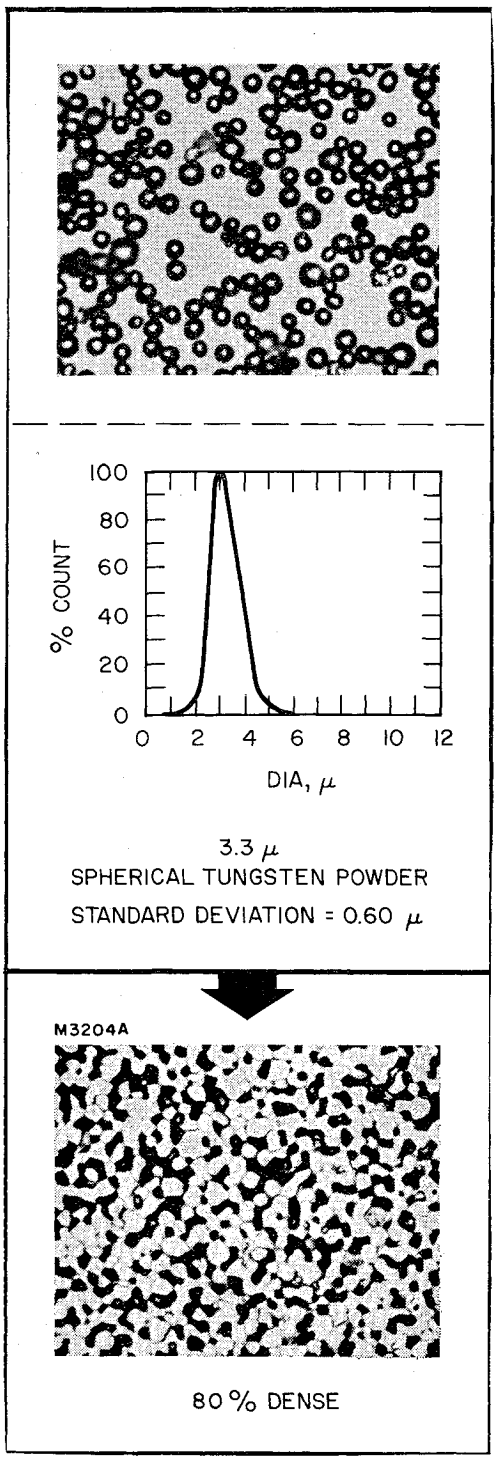

Fig. 1 Classified 3.3 μ spherical tungsten powder, its size distribution, and the resulting sintered porous structure; 750×.

Results are evaluated here according to the methods used by Jordan and Duwez[2] and Kothari.[3] A dimensionless densification parameter δ may be computed from D_s, D_p, and ρ, the sintered density, pressed density, and absolute density, respectively, where

$$\delta = (D_s - D_p)/(\rho - D_p)$$

This parameter is plotted vs log sintering time for the two powders in Fig. 3. Variations from a straight line over the short-time portions of the curves may have resulted partly from experimental difficulties in obtaining accurate short-time high-temperature conditions.

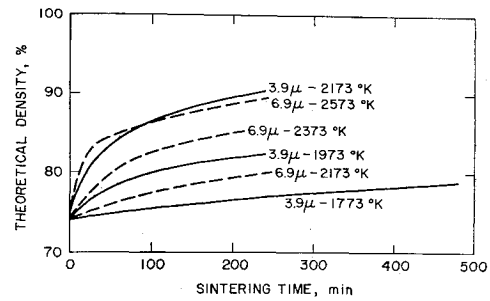

Fig. 2 Pellet densification for 3.9- and 6.9-μ spherical tungsten powders.

Values of constant δ are plotted on a graph of $1/T$ (°K) vs log sintering time (Figs. 4a and 4b) where straight lines are obtained. This indicates a simple rate process behaving according to the following Arrhenius-type relation:

$$\ln(t_1/t_2) = Q/R[(1/T_1) - (1/T_2)]$$

where R is the gas constant, and Q is the activation energy of the sintering process. Since the slope of these lines is $Q/2.3\,R$, the activation energies may be calculated for each value of δ (Fig. 5).

The sintering of tungsten powder may be considered to occur by three modes of diffusion: surface diffusion, with an activation energy of 65 kcal/mole; grain boundary diffusion (90 kcal/mole); and volume diffusion (140 kcal/mole).[3] The curves of activation energy vs density (Fig. 5) show, by the increase of activation energy with sintering, that the mode of diffusion is changing through at least the first two stages mentioned previously. It is interesting to note that the finer powder starts lower (as expected because of its higher surface area) but reaches a higher value of activation energy for the same density as the coarse powder. This is indicative of the change in structure from large pores, high internal surface area, and short grain boundaries to small pores, low internal surface area, and longer grain boundaries.

Direct count of surface pores shows a linear relationship between pore density and density of the porous material (Fig. 6), over the range of 76 to 91% dense. Note that the 2.4-μ material, which sinters more rapidly than the 3.9- or 6.9-μ material, is less valuable for long-term operation because of its decrease in porosity. Above densities of 85%, closure of many pores is expected in the finer powders, although the

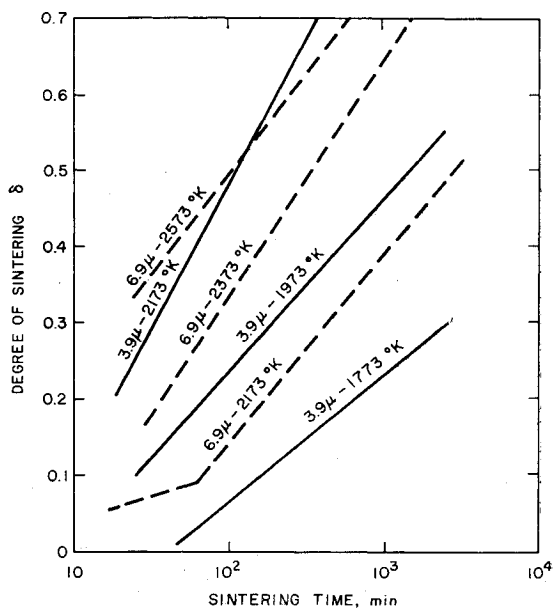

Fig. 3 Degree of sintering δ of the 3.9- and 6.9-μ spherical tungsten powders.

spherical material exhibits remarkable preservation of interconnectability.

Kothari[3] tested commercial tungsten powder in the 3-μ size range; this powder had a wider size distribution than that tested for the present study. At sintering temperatures from 1373° to 1773°K, he found that grain boundary diffusion was the prevalent mode of sintering. The present values average in the grain-boundary-diffusion range. Comparison with the present study is difficult because of size differences, the lack of fine powder fraction in the classified material (this affects sintering rate considerably), and the higher and wider range of temperatures studied.

The constant δ lines in Figs. 4a and 4b may be considered as constant density lines, since pressed density D_p varies so little. Extrapolation of these lines to ionizer operating temperatures and durations of one year (admittedly an inaccurate extrapolation considering the short sintering times of the present study) permits an approximation as to the stability of the material. The time differential between any two density lines at a constant temperature is a measure of the time required for the change in density to occur. It can be seen that the 3.9-μ material at 1473°K and a density of 81.8% would require 8 to 9 yr to densify to 84.4%.[4-6] The same material at the same temperature would require only 9 months to densify from 79.2 to 81.8%. This method may be used to predict both high- and low-temperature stability.

Using known data of time stability and coupling these with operating temperatures, ionizer pore densities may be fabricated for predictable lifetimes. It is expected to extend the present work to longer sintering times (up to two months), lower temperatures, different powder sizes and distributions, and to typical commercial powders.

Electrical Characteristics of Porous Tungsten Pellets

The electrical characteristic of porous ionizers, besides depending on the pore density, strongly depends on the ionizer surface condition. In particular, oxygen and carbonaceous gases change neutral flux and critical temperature. All of the measurements reported here therefore have been made in ultrahigh vacuum to simulate space conditions.[1,7] The system is pumped by a 200 liter/sec ion pump after baking at

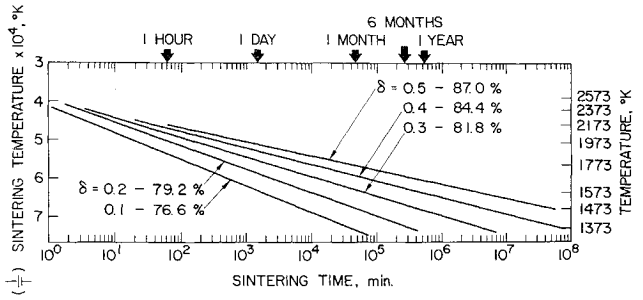

Fig. 4a) 3.9-μ spherical tungsten powder sintering time vs $1/T$ (constant δ lines).

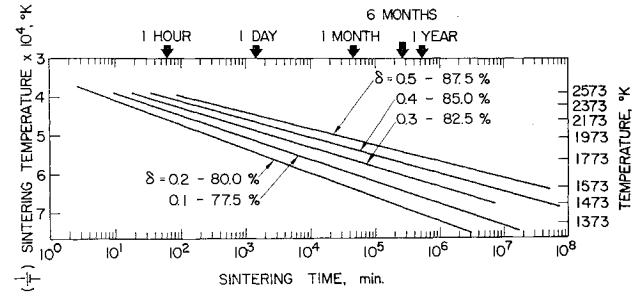

Fig. 4b) 6.9-μ spherical tungsten powder sintering time vs $1/T$ (constant δ lines).

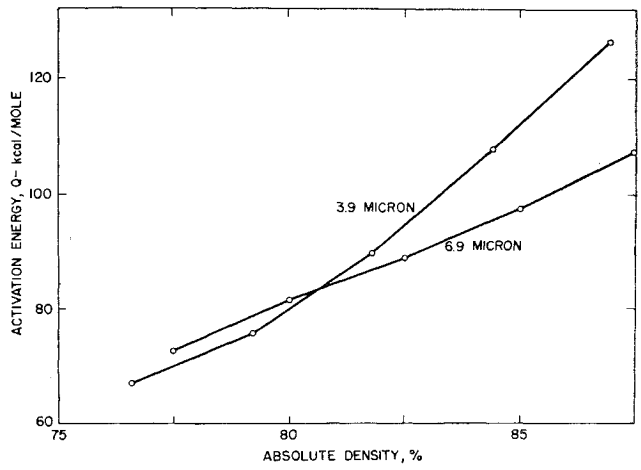

Fig. 5 Tungsten powder sintering activation energy depending on the pellet density (percent of theoretical density).

150°C for 12 hr. A pressure of 10^{-6} torr is maintained during baking by a mercury diffusion pump, which is separated from the mechanical pump by a zeolite trap. Prior to the measurements, the total pressure is in the low 10^{-9} torr range. Typical mass spectra (mass number range from 2 to 80) reveal only small amounts of water vapor and some hydrogen.[8] Partial pressures of oxygen and the hydrocarbons, below 10^{-10} torr, are beyond the range of the Consolidated Electric Dynamics Company (CEC) 21-612 residual gas analyzer employed here.

The emitter Richardson work function is measured prior to the ion beam experiments in order to check surface conditions. This measurement is repeated frequently during the pellet evaluation. At first, the electron work function generally exceeds that of clean tungsten, but the surface is usually cleaned by heating the pellet above 1600°K. If the work function is below that of clean tungsten, oxygen with a partial pressure close to 10^{-5} torr is added (only for the time carbon monoxide is indicated by the mass spectrometer). If volume carburization is evident, the pellet is discarded. Application of high-temperature and small cesium flow rates usually clean the pellet in a few hours. A clean surface is indicated by a Richardson plot with work function 4.55 ± 0.05 eV and, with A = 120 a/cm² deg², usually measured over a 1200° to 1700°K temperature range.

At ion current densities exceeding several milliamperes per square centimeter, a tendency toward high voltage discharges is frequently observed. The discharge is sensitive to dust particles and cesium. To reduce the amount of cesium, the acceleration electrode has been built in two layers: the layer opposite the emitter is externally heated to operate in the

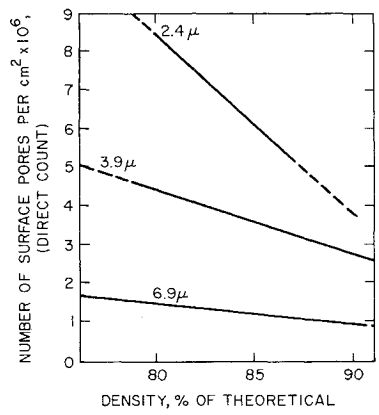

Fig. 6 Relation between number of surface pores per cm² (per direct count) and the pellet density for three spherical tungsten powders.

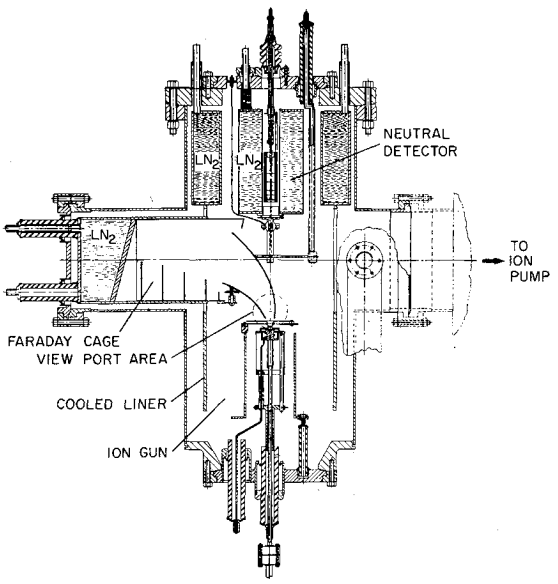

Fig. 7 Cross section of pellet evaluation test tube.

minimum of the electron emission S curve, and the upper layer, which faces the neutral detector, is water cooled.

Ion beam interception by the acceleration electrode is negligible. Contribution of charge exchange ions to secondary electron emission from this electrode yields less than 0.1% to ion current reading. The electrostatically deflected ion beam is completely intercepted by the Faraday cage. This is confirmed by the sputtering pattern inside the titanium lined and LN_2 cooled cup. The outer deflection plate carries side shields in order to reduce beam expansion normal to the drawing plane (Fig. 7). Further, in the space charge limited range, the ion beam does not expand with increasing ion current because $r_2/r_1 = \text{const}\ x(i/U^{3/2})^{1/2} = \text{const}\ xp^{1/2}$ with $i = p \times U^{3/2}$. p is the ion gun perveance, U is the acceleration potential, and r_2 and r_1 are the ion beam radii at the cage and the acceleration electrode. The ion gun structure temperature compensated, and the perveance is independent of the ion current. The neutral flux is measured opposite to the ion emitter, and these measurements are independent of the deflected ion beam. The signal-to-noise ratio is optimized because of the collimator design.[1,9] The collimator is optically and electrically aligned from outside of the vacuum chamber. Change in neutral efflux characteristic from a cosine distribution may be measured through a change in the neutral detector geometry factor (the ratio of total neutral efflux at zero acceleration potential to the fraction of neutral flux indicated by the neutral detector ND). In the case of cosine distribution, the geometrical factor is $A/R^2\gamma = 1/14{,}190$, with A the collimator cross section and $R = 18.9$ cm, the distance between ion emitter and ND anode.

As has been pointed out earlier by one of the authors, the cesium neutral efflux depends on the cesium flow rate per pore.[1] The pore size appears to have little effect on the neutral efflux up to ion current densities of at least 10 ma/cm² and pore densities of 10^6 pores/cm² (by the line intercept or traverse technique[10,11]). This resulted from pellet investigations, covering pore radii between 5 and 1.0 μ.[1] The conclusion regarding pore size and neutral efflux is further emphasized by the investigation of two pellets from the same tungsten billet, one with both surfaces chemically etched and the other with both surfaces highly polished. The surfaces were prepared prior to copper removal. Under clean surface conditions the neutral flux was equal for both of the pellets, inside the 0.3% error limit. Both of the pellets have 9.6×10^5 pores/cm², but different pore sizes.

Surface roughness may become important at higher current densities, to avoid overlapping emission centers. With 10^7 equally spaced pores/cm², the maximum emission radius is 1.58 μ for each center. The average surface migration length is proportional to the square root of the surface diffusion coefficient and the average absorption time. Because the temperature-dependent surface diffusion coefficients for cesium atoms and ions are unknown, an estimate of the actual emission center size is difficult. According to preliminary ion microscope studies with Cs on porous tungsten, the emission center radius is in the 1 to 2μ range at higher flow rates per pore. Theoretical considerations of other investigators[12] consider both the pore size and pore distance as the neutral efflux governing parameters.

It was stated earlier that charge exchange has negligible effect on the neutral efflux measurement.[1] The charge exchange effect is discussed below in greater detail. Various investigators have reported a charge exchange cross section σ for cesium of about 2.35×10^{-14} cm² at 5 kv,[13] and the number of charge exchange neutrals per square centimeter per second is

$$N = (\sigma n \bar{j} L/v \cdot e)\gamma A$$

where n is the neutral efflux/cm²-sec; $\bar{j}$ is in amperes per square centimeter, L is the length (in centimeters) of interaction between ion and neutral beams (here 90% of the interactions are considered because of the ion beam deflection); v is the thermal velocity of the neutrals ($v = 1.455 \times 10^4 (T/M)^{1/2}$ cm-sec^{-1}), with T the emitter temperature in degrees Kelvin and M the atomic mass number ($e = 1.6 \times 10^{-19}$ C); A is the neutral detector collimator cross section with 8×10^{-2} cm²; and γ depends on the observed scattering angle of the charge exchange process.

The average ion current density in the interaction volume must be considered in connection with the ion beam expansion. The average ion beam cross section $\bar{F} = 1.37$ cm² where $F_1 = 0.25$ cm² and $F_2 = 2.5$ cm² and $\bar{j} = 1.83$ ma/cm² at the emitter ion current density of 10 ma/cm². The distance L between F_2 and F_1 depends on the ion beam expansion with $r_2/r_1 = (4.1 \times 10^6 M^{1/2} j L^2/U^{3/2})^{1/2}$,[14] where r_1 is the radius of F_1 and U the acceleration potential. Because of cosine distribution, the neutral flux per square centimeter is

$$n = n_0 \cdot A^*/r^2\pi$$

in the ion-neutral interaction volume, with $r = L/3$ somewhat overestimating n; A^* is the emitter surface area with 0.25 cm², and n_0 is the neutral efflux per square centimeters from the emitter surface. We still must consider the angular distribution of the charge exchange neutrals. Because the de Broglie wavelength ($\lambda = h/mv$) of cesium is much smaller

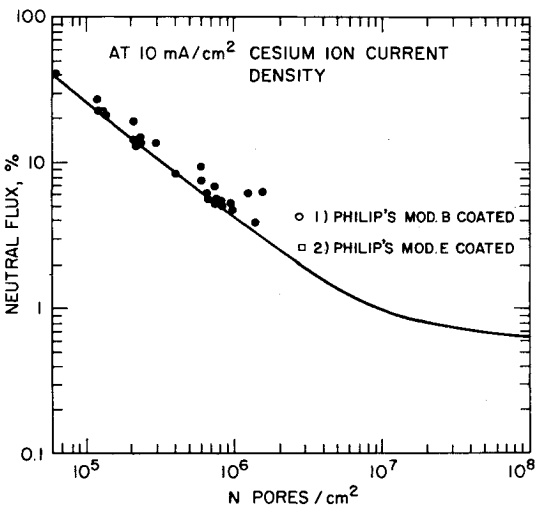

Fig. 8 Neutral efflux from porous tungsten at 10 ma/cm² cesium ion current density vs the pore density per cm² (traverse counting technique).

Table 1 Pellet data

Pellet	Transmission coefficient	Pellet density, %	Coat density, % and thickness	Average pore size, μ	Average pore distance, μ	Line intercept pore density/cm^2
HRL ZW-2.8 sp-4	4.25×10^{-5}	81.5	...	1.6	5.6	1.9×10^6
Mod. E, coat	8.2×10^{-5}	74	70%, 5 mils	2.23	3.89	2.7×10^6
Mod. B, coat	1×10^{-4}	80	70%, 5 mils	2.23	3.89	2.7×10^6
Mod. E, polished	3.0×10^{-4}	72	...	2.4	7.8	9.7×10^5
Mod. E, etched	3.0×10^{-4}	72	...	2.4	7.8	9.7×10^5
Mod. B	1.8×10^{-4}	81.5	...	3.6	17.3	2.27×10^5

than the dimension of the scattering body, and small angle scattering is predominant,[15] the differential scattering cross section σ varies strongly with the scattering angle θ. Approximately all of the charge exchange neutrals are deflected into an angle of $\pm 8°$ relative to the neutral detector axis,[15] but only those with a deflection angle of less than $1.88° \times 10^{-2°}$ pass the collimator. If $\sigma(\theta)$ is approximated by the error function, we have

$$\sigma(\theta) = \sigma_0 \exp - \theta^2$$

and

$$\xi = 2\pi \int_0^\theta \sigma(\theta) \sin\theta \, d\theta$$

With $\theta = 1.88 \times 10^{-2}$ degree, it follows from the series development

$$\xi = \pi\sigma_0\theta^2$$

and

$$\gamma = \pi\theta^2 = 1.1 \times 10^{-3}$$

For an emitter ion current density of 10 ma/cm^2, with 4% neutral efflux (10^6 pores/cm^2), the contribution of charge exchange neutrals to the neutral detector current is negligible, because 3.97% of the neutral efflux comes from the emitter, and only 0.03% is contributed by the charge exchange process.

According to the Saha-Langmuir equation, the neutral flux depends to some extent on the pellet temperature. It is at its minimum at critical temperature and increases with T. Measuring the neutral flux at constant ion emitter temperature over the whole range of current densities leads toward too high neutral flux at the low current densities. Below 1 ma/cm^2, the neutral flux approaches that of solid tungsten.

The pore density per unit surface area has been measured by the traverse technique.[10] On photomicrographs, the traverses are spaced so that each pore is counted only once. The average pore size and distance are computed from the corresponding traverse intersections. The traverse technique allows one to transfer the average pore diameter and the average pore distance directly into the corresponding volumes of the species, if the statistic is large enough. In order to keep the relative statistical error below 3%, more than 10^3 counts/pellet have been evaluated.

The relation between current density, neutral efflux, and pore density on tungsten in the range up to 10 ma/cm^2 is approximated by

$$\log(100 - \beta^*) = 0.8 \, (\log j + 8.75 - \log N)$$

with β^*, the ionization efficiency, in percent; j in amperes per square centimeter; and N the pore density per square centimeter. This equation is in close agreement with that published earlier,[1] and its error limit does not exceed 0.3%.

Figure 8 presents neutral efflux data as a function of pore density for a number of tungsten pellets. The number of open pores corresponds with the counted pore density only for part of these pellets. In Fig. 8, (1) and (2) indicate coated pellets. Various pellets with pore counts between 2×10^5 and 3×10^6 pores/cm^2 are compared in Table 1 to explain the improvement in performance as a result of surface coat. The influence of the substrate pore density on the neutral efflux of the coated pellets is evident from Fig. 8, because both pellets have a 5-mil-thick coat made from the same 2.4-μ spherical tungsten powder (such as the Hughes Research Laboratories (HRL) ZW 2.8 sp-4 uncoated pellet). Figure 9 shows the cross section of this HRL pellet and the coated material. Magnifications are 2000 and 500, respectively. The neutral flux from the modification B pellet reaches 10% at 6 ma/cm^2 cesium ion current density when uncoated (Fig. 10). Coating this substrate with a 5-mil layer of spherical tungsten powder with 2.4-μ grain size and a layer density close to 70% reduces the neutral flux to 2.1% at the same current density. Higher pore density of the base material further reduces the neutral flux from its coated surface, as indicated in Fig. 10 for coated Mod. E material. At a 10 ma/cm^2 current density, the neutral flux is 2.7%.

Curves for uncoated tungsten with 10^6 and 3×10^6 pores/cm^2 are included. Their slope is less steep than that of

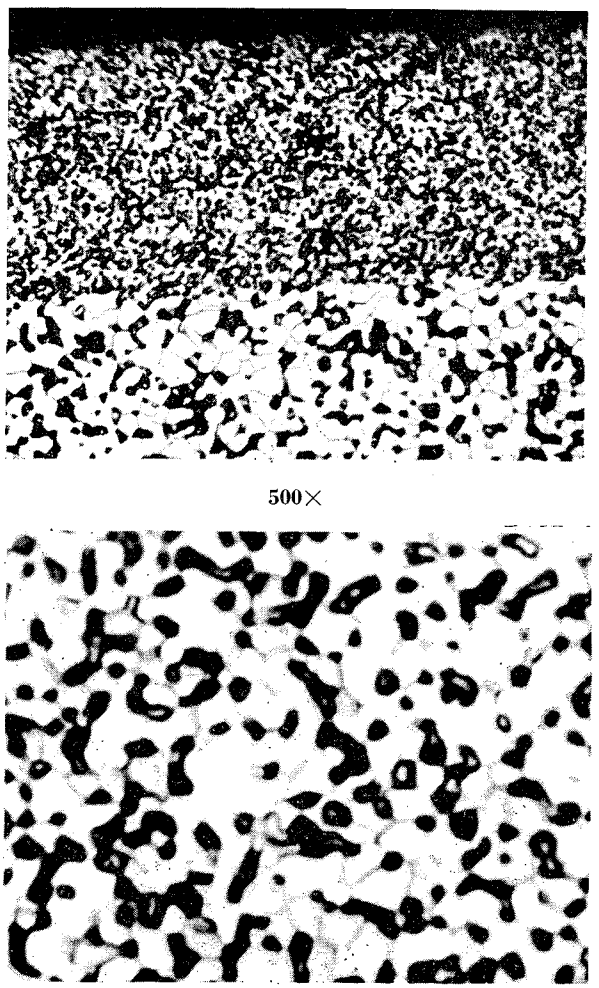

500×

2000×

Fig. 9 Cross section of coated tungsten substrate and the 2.4-μ spherical tungsten pellet.

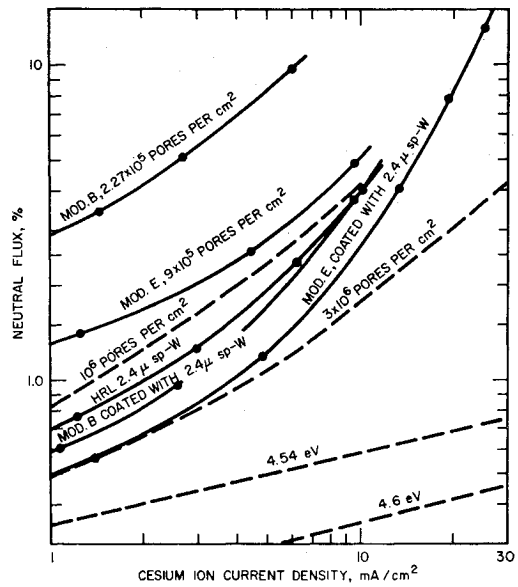

Fig. 10 Comparison of high pore density uncoated and coated tungsten pellets.

the coated materials and we may therefore assume that the coated pellets will further improve with coat thickness. As expected, the ion current vs neutral flux from the HRL pellet is less steep as compared with the coated materials; this is important in connection with high current densities. Further increase of the pore density lowers neutral flux, particularly at current densities exceeding 10 ma/cm², as indicated by the extrapolated curve with 3×10^6 pores/cm². The neutral efflux of the HRL pellet is 4% at 10 ma/cm². Data from the Mod. E coated material show that neutral flux below 5% at 15 ma/cm² ion current density is possible; maximum current densities of 25 ma/cm² have been measured for this material with 13.3% neutral flux. (Other investigators[16] report lower neutral efflux data from different porous tungsten.)

Ion current densities exceeding 25 ma/cm² can be achieved without difficulty. High voltage breakdown depends on the total, rather than the relative number of cesium atoms leaving the emitter surface. Therefore, reducing the emitter surface area from its original size of 0.25 cm² permits higher current densities than are reported here, and 50 ma/cm² is not the upper limit. The critical temperature for cesium ionization on porous tungsten with 10^6 pores/cm² is[1]

$$T_c = [12{,}500/(7.37 - \log i)]^\circ\text{K}$$

The emitter radiation losses in connection with cesium ionization decrease strongly in the pore density range between 10^5 and 10^6 pores/cm² and approach asymptotically the value for solid tungsten at higher pore densities.[1] This is similar to the decrease of neutral flux with pore density. Therefore, increased pore density improves over-all efficiency of the ion engine, i.e., the product of power and ionization efficiencies. In addition, the ion engine lifetime increases remarkably with the ionizer pore density.

Conclusions

Experiments proved that the neutral flux can be kept below 5% at 15 ma/cm² cesium ion current density. Under this condition, the critical temperature exceeds that of solid tungsten by 32°K. For successful operation of surface ionization type ion engines, pore densities exceeding 10^6 pores/cm² are necessary. Figure 6 indicates a fairly strong decrease in pore density vs time for the 2.4-μ spherical tungsten powder; the 3.9-μ spherical tungsten powder exhibits a reasonable stability, and larger grain sizes of the highly classified material exhibit improved performance. Pore densities of 10^7 pores/cm² (by the traverse technique) are desirable. For further improvement of the ionizer, we recommend a study of other materials, refractory metals and alloys, that have higher work functions than that of polycrystalline tungsten, and if possible, lower critical temperature (connected with improved sintering characteristics). Incorporation of porous pellets with a rhenium coating may further improve the ion engine characteristics.

References

[1] Husmann, O. K., "A comparison of the contact ionization of cesium on tungsten with that of molybdenum, tantalum, and rhenium surfaces," AIAA J. **1**, 2607–2614 (1963).

[2] Jordan, C. B. and Duwez, P., J. Metals, **1**, 96 (1949).

[3] Kothari, N. C., "Sintering kinetics in tungsten powder," J. Less-Common Metals **5**, 140–150 (1963).

[4] Anglin, A. E., Jr., "Problems of porous tungsten ionizers for cesium electric propulsion systems," National Society of Aerospace Material and Process Engineers Spring Symposium on Space Power Systems Materials, Philadelphia, Pa. (June 1963).

[5] Jones, W. D., *Fundamental Principles of Powder Metallurgy* (Edward Arnold and Co., London, 1960).

[6] Leszynski, W., *Powder Metallurgy* (Interscience Publishers, Inc., New York, 1961).

[7] Husmann, O. K., Jamba, D. M., and Denison, D. R., "The influence of residual gas atmosphere in space chambers on the neutral efflux and the critical temperature of tungsten ionizers," AIAA Preprint 64-693 (1964).

[8] Riviere, J. C. and Allinson, J. D., "Gas evolution during baking of sputtering ion pumps," Vacuum **14**, 97–102 (1964).

[9] Ruth, V., Winterbottom, W. L., and Hirth, J. P., "Die Winkelabhaengigkeit der mit einer Knudsenzelle erzeugten Molekularstrahlen," Z. Angew. Phys. **16**, 53–55 (1963).

[10] Muenzer, H. and Schneiderhoehn, P., "Das Sehnenschnitt verfahren," Heidelberger Beitr. Mineral. Petrog. **3**, 456–471 (1953).

[11] Husmann, O. K., "Diffusion of cesium and ionization on porous tungsten," *AIAA Progress in Astronautics and Rocketry: Electric Propulsion*, edited by D. Langmuir, E. Stuhlinger, and J. Sellen Jr. (Academic Press, New York, 1961), Vol. 5, pp. 505–521.

[12] Nazarian, G. M. and Shelton, H., "Theory of ion emission from porous media," *AIAA Progress in Astronautics and Rocketry: Electric Propulsion*, edited by D. Langmuir, E. Stuhlinger, and T. Sellen Jr. (Academic Press, New York, 1961), Vol. 5, pp. 91–106; also, Reynolds, T. W. and Kreps, K. W., "Gas flow, emittance and ion current capabilities of porous tungsten," NASA TND-871 (1961).

[13] Marino, L. L., Smith, A. C. H., and Caplinger, E., "Charge transfer between positive cesium ions and cesium atoms," Phys. Rev. **128**, 2243–2250 (1962).

[14] Von Ardenne, M., *Tabellen zur Angewandten Physik* (VEB Deutscher Verlag der Wissenschaften, Berlin, 1964), Vol. 1, p. 619.

[15] Massey, H. S. W. and Mohr, C. B. O., "Free path and transport phenomena in gases and the quantum theory of collisions: I. The rigid sphere model," Proc. Roy. Soc. **A141**, 434 (1933).

[16] LaChance, M., Kuskevics, G., and Thompson, B., "High-performance cesium ionizers made from sized spherical tungsten powder," AIAA J. **3**, 1498–1505 (1965).